Allosteric Inhibition as a New Mode of Action for BAY 1213790, a Neutralizing Antibody Targeting the Activated Form of Coagulation Factor XI

Martina Schaefer[1], Anja Buchmueller[2], Frank Dittmer[3], Julia Straßburger[2] and Andreas Wilmen[4]

*1 - **Bayer AG,** Research and Development, Pharmaceuticals, Structural Biology, 13342 Berlin, Germany*
*2 - **Bayer AG,** Research and Development, Pharmaceuticals, Cardiovascular, 42096 Wuppertal, Germany*
*3 - **Bayer AG,** Product Supply, Pharmaceuticals, Quality Control, 51368 Leverkusen, Germany*
*4 - **Bayer AG,** Research and Development, Pharmaceuticals, Protein Engineering and Assays, 50829 Cologne, Germany*

Correspondence to Martina Schaefer: *martina.schaefer1@bayer.com*
https://doi.org/10.1016/j.jmb.2019.09.008
Edited by Sachdev Sidhu

Abstract

Factor XI (FXI), the zymogen of activated FXI (FXIa), is an attractive target for novel anticoagulants because FXI inhibition offers the potential to reduce thrombosis risk while minimizing the risk of bleeding. BAY 1213790, a novel anti-FXIa antibody, was generated using phage display technology. Crystal structure analysis of the FXIa−BAY 1213790 complex demonstrated that the tyrosine-rich complementarity-determining region 3 loop of the heavy chain of BAY 1213790 penetrated deepest into the FXIa binding epitope, forming a network of favorable interactions including a direct hydrogen bond from Tyr102 to the Gln451 sidechain (2.9 Å). The newly discovered binding epitope caused a structural rearrangement of the FXIa active site, revealing a novel allosteric mechanism of FXIa inhibition by BAY 1213790. BAY 1213790 specifically inhibited FXIa with a binding affinity of 2.4 nM, and in human plasma, prolonged activated partial thromboplastin time and inhibited thrombin generation in a concentration-dependent manner.

Introduction

Anticoagulants are the cornerstone of the prevention and treatment of thrombotic disorders, but those in current clinical use are associated with a dose-dependent risk of bleeding, which limits their antithrombotic potential. Warfarin, a vitamin K antagonist, has been used for decades, but has a narrow therapeutic window, necessitating close monitoring and frequent dose adjustments to minimize side effects associated with an increased risk of bleeding (e.g., gastrointestinal bleeding). Fixed-dose non-vitamin K antagonist oral anticoagulants, which directly target enzymes in the coagulation cascade such as thrombin or factor Xa (FXa), are also effective and are associated with a lower risk of some types of bleeding than warfarin [1]. However, further reduction in the risk of bleeding remains desirable [2].

Factor XI (FXI) is a potential alternative therapeutic target in the coagulation cascade [3]. It is the zymogen of the serine protease activated FXI (FXIa) which contributes to thrombin generation and fibrin formation via activation of factor IX (FIX) [4]. FXI has been shown to be activated by thrombin and FXI itself, in addition to activated factor XII (FXIIa) [5]. FXIa then amplifies thrombin generation and contributes to fibrin stabilization via the sequential activation of FIX and factor X [5−7]. As such, FXI represents an attractive target because it contributes to thrombosis but plays only a minor role in hemostasis [8,9]. Human epidemiological data and animal studies support the potential of FXI inhibition as an antithrombotic strategy. Individuals with congenital FXI deficiency appear less prone to ischemic stroke and venous thromboembolism (VTE) than the general population and do not appear to have a consistently increased bleeding tendency [10−13]. Conversely, observational studies have suggested that elevated FXI activity may be associated with a greater prevalence of ischemic stroke or VTE [14−17].

In animal studies, reduction of FXI using knockout strains, antisense oligonucleotides (ASOs) that

inhibit FXI synthesis in the liver, or monoclonal antibodies that inhibit FXI activation or activity, have shown protection against induced arterial and venous thrombus formation without increased risk of bleeding [18–29]. An ASO known as IONIS-416858 (now IONIS FXI_{Rx} or BAY 2306001) was the first agent targeting FXI/FXIa to be evaluated in humans, in a phase 2 multicenter randomized trial for VTE prevention in patients undergoing total knee arthroplasty [30]. Lowering FXI levels reduced the risk of postoperative VTE compared with administration of enoxaparin, a parenteral anticoagulant commonly used in this setting, without significantly increasing bleeding risk [2,30].

Small molecule inhibitors of FXI/FXIa, acting by orthosteric [31–36] or allosteric [37–39] mechanisms, have also been developed. The availability of X-ray crystal structures of the FXIa catalytic domain (FXIa-CD) has contributed to ligand-based and structure-based drug design [40,41]. FXI is a homodimer of 80-kDa subunits, each containing four amino acid repeats called apple domains and a C-terminal trypsin-like catalytic domain [42–44]. The catalytic domain active site contains the catalytic triad of His413, Asp462, and Ser557, and subsites responsible for substrate selectivity (S4–S3–S2–S1–S1′–S2′–S3′–S4′). In addition, the catalytic domain contains an anion or heparin binding site, through which heparin can inhibit FXIa allosterically [4,42,45–47]. The four apple domains (A1–A4) contain binding sites for other proteins, for example, A1 for thrombin [48], A2 for high-molecular-weight kininogen [49], A3 for FIX [50], glycoprotein Ib [51] and heparin [52,53], and A4 for FXIIa [54]. Cys321 of the A4 domain forms an interchain disulfide bond with Cys321 in the A4 domain of a second subunit leading to the dimeric structure, unique among coagulation proteases [55,56]. Hydrophobic residues, including Leu284, Ile290, and Tyr329 of the A4 domain interface and the salt bridges between Lys331 and Glu287 of each monomer, are also required for homodimer formation [4,42,45]. Activation of FXI subunits involves proteolysis of the Arg369–Ile370 bond, catalyzed by FXIIa or thrombin [5,57,58]. After activation, the free N-terminus of FXIa can move towards the activation pocket, creating the oxyanion hole necessary for catalytic activity. The 3D architecture of FXI, based on a structure published by Papagrigoriou et al. is shown in Fig. 1 [59].

The aims of this study were to generate a neutralizing monoclonal antibody against FXIa using phage display technology to study the nature of its interaction with FXIa and to assess its anticoagulant properties *in vitro*.

Results

Screening of 50 000 antigen-binding fragment variants led to the selection of BAY 1213790

Antigen-binding fragments (Fabs) directed against human and rabbit FXI and FXIa were identified by panning a phage-displayed fully human antibody library [60]. Ultrahigh-throughput screening techniques were used to screen the library for candidate Fabs. Of 50 000 Fab variants screened, 4800 variants were selected for evaluation in FXI and FXIa biochemical activity assays (Fig. S1). In the latter assays, the proteolytic activity of FXIa was indicated by its ability to cleave a generic substrate (with a quencher moiety and a fluorogenic substrate separated by a cleavage site of three amino acids), resulting in the release and detection of a fluorogenic group. Consequently, any inhibition of FXIa activity by function-blocking antibodies resulted in a reduction in signal intensity. Based on their inhibitory activity, 1100 candidates were submitted for genotypic characterization sequencing, which identified 198 clones with unique sequences in their complementarity-determining regions (CDRs). These hits were recloned to generate full-length antibodies and selected for subsequent recombinant expression and purification.

Of these 198 candidates, BAY 1184816 showed the highest function-blocking activity but an extremely low expression rate (70 mg/L). To improve the

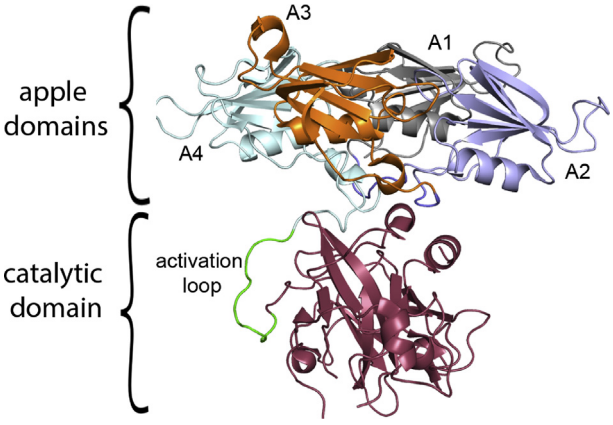

Fig. 1. 3D architecture of FXI based on PDB entry 2F83 [59]. The four apple domains are on the top and are colored gray (A1), purple (A2), orange (A3), and cyan (A4). The activation segment, which is cleaved by FXIIa, thrombin or FXIa, is highlighted in green. The catalytic domain is depicted in maroon. After cleavage the new N-terminus of FXIa moves toward the active site, forming the oxyanion hole and allowing proper orientation of the catalytic triad.

expression rate, certain positions of amino acids within the CDRs were randomly selected and exchanged to a different amino acid. Substitution of the amino acid Asp110Asn within the CDR loop 3 produced BAY 1213790, resulting in a significant increase of approximately fourfold in the expression level from transient transfected human embryonic kidney 293 (HEK293) cells (>300 mg/L).

BAY 1213790 functionally neutralized FXIa activity with high selectivity, specificity, and affinity

Selectivity of BAY 1213790

BAY 1213790 was tested for selectivity against a serine protease panel that included thrombin, FXa, FVIIa, FXIa, trypsin, plasmin, tissue plasminogen activator, and kallikrein. At concentrations of up to 10 μM, BAY 1213790 did not show any inhibitory activity on these proteases (Fig. S2).

Specificity and affinity of BAY 1213790

BAY 1213790 bound specifically to human FXIa with a half-maximal effective concentration (EC_{50}) of 0.2 ± 0.02 nM (n = 4) (Fig. 2a). Binding of BAY 1213790 to FXI was not detected.

To test if FXIa-CD (Cys500Ser mutant, amino acids 388–625) might be well suited for cocrystallization and to narrow down the binding epitope for BAY 1213790, the affinity (KD) of BAY 1213790 for human FXIa-CD was determined using surface

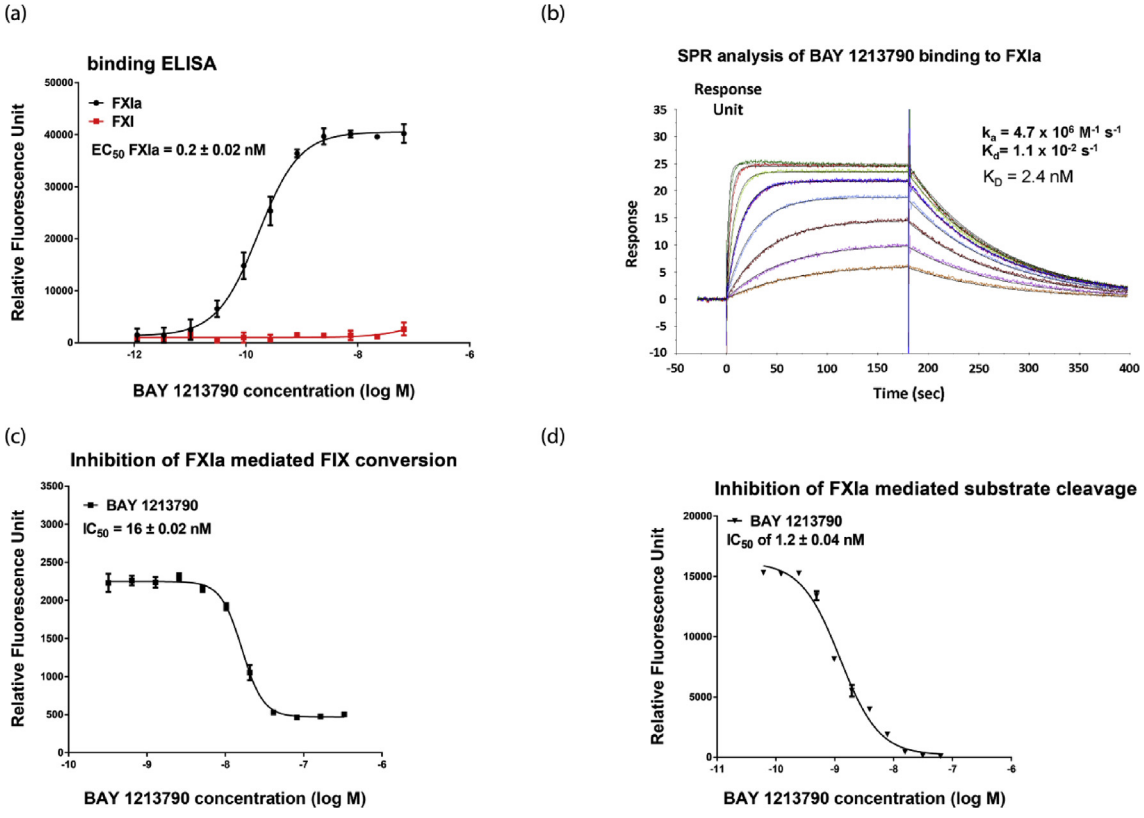

Fig. 2. Specificity and Affinity Testing of BAY 1213790 and Functional Neutralization of FXIa. (a) Binding of BAY 1213790 to human FXI and FXIa determined by standard ELISA procedure. FXIa and FXI, respectively, were coated to Maxisorp microtiter plates. Binding activity of BAY 1213790 was detected by using an anti-h-Fc-POD antibody. Excitation and emission wavelengths were 535 and 590 nm, respectively. Data were analyzed by using GraphPad Prism software and are presented as mean ± standard error of the mean, n = 4. (b) SPR sensorgrams of immobilized BAY 1213790 depicting binding analysis to human FXIa-CD. The colored traces denote experimental data and black traces denote fitted data. (c) Functional neutralization of FXIa by BAY 1213790 in human plasma as measured by inhibition of conversion of the natural substrate FIX to FIXa. Human plasma was diluted in buffer to a final concentration of 30%. Various concentrations of BAY 1213790 were added to the diluted plasma and incubated for 30 min. The activity of FIXa was measured by adding a specific fluorogenic substrate for FIXa. Data were analyzed using GraphPad Prism software. All experiments were performed four times and data are given as mean ± standard error of the mean. (d) Functional neutralization measured by cleavage of a specific fluorogenically labeled substrate of FXIa in human plasma. Data are presented as mean ± standard error of the mean, n = 4.

plasmon resonance (SPR). The KD was calculated to be 2.4 nM, based on an association rate constant (ka) of 5.4 $\times$ 10^6 M^{-1} s^{-1} and a dissociation rate constant (kd) of 1.3 $\times$ 10^{-2} s^{-1}. The fit for the experimental data had a χ [2] value of 2.14 (Fig. 2b).

Functional Neutralization of FXIa by BAY 1213790

BAY 1213790 inhibited FXIa-mediated activation of FIX (the natural substrate of FXIa) in human plasma with a half-maximal inhibitory concentration (IC_{50}) of 16 $\pm$ 0.02 nM (n = 4) (Fig. 2c); FXIa-induced cleavage of a specific, fluorogenically labeled substrate in human plasma was inhibited with an IC_{50} of 1.2 $\pm$ 0.04 nM (n = 4) (Fig. 2d).

A network of favorable interactions at the interface between FXIa-CD and the Corresponding Fab Fragment of BAY 1213790 stabilized the whole complex

To understand the detailed mechanism of antagonism of FXIa by BAY 1213790, a 2.7 Å crystal structure of the complex consisting of human FXIa-CD and the corresponding Fab fragment of BAY 1213790 (BAY 1213790-Fab) was obtained (Fig. 3a and b). Data collection statistics and refinement results are summarized in Table S1. The FXIa–BAY 1213790-Fab complex crystallized in the orthorhombic space group $P2_122_1$ with only one copy of the complex per asymmetric unit. BAY 1213790-Fab showed the typical immunoglobulin fold and CDR loops of the heavy chain (VH), and the light chain (VL) of the Fab participated in binding to FXIa-CD (Fig. 3a and b).

A network of favorable interactions at the interface between BAY 1213790-Fab and FXIa-CD stabilized the whole complex (Fig. 3c). The tyrosine-rich CDR loop 3 of the VH penetrated deepest into the FXIa-CD epitope, with Tyr102 on the loop tip forming a direct hydrogen (H)-bond to the sidechain of Gln451 (2.9 Å). In addition, pi–sigma interactions with C_α of Arg413 (not visible in Fig. 3c) were observed, as well as a strong π–π T-shaped intramolecular interaction with neighboring Tyr103. Tyr103 itself was pi-stacked to the peptide plane of Gln451/Ser452. Tyr104 of CDR loop 3 was involved in intramolecular π–π stacking to Tyr51 of the VL, and Tyr105 of CDR3 was involved in H-bonding to Asp35 of CDR1 in the VH, stabilizing its orientation and the overall architecture of the Fab. Further intramolecular H-bonds from the ammonium group of Lys527 to the main chain carbonyl of Gly99 and Gly100 of CDR3 and from the amide of Tyr103 to the carbonyl of Lys527 completed the strong interaction pattern found for CDR3. The tip of the loop of CDR1 of the VH only interacted with FXIa-CD via van der Waals contact and the only residue to interact was Asp35, which formed a salt bridge to Arg525 of FXIa-CD (Fig. 3c). The CDR2 of the VH did not contribute to binding of the Fab to FXIa-CD. Because of the number and nature of interactions of CDR loop 3 of VH to BAY 1213790 it can be speculated that this contribution might be most important for binding of

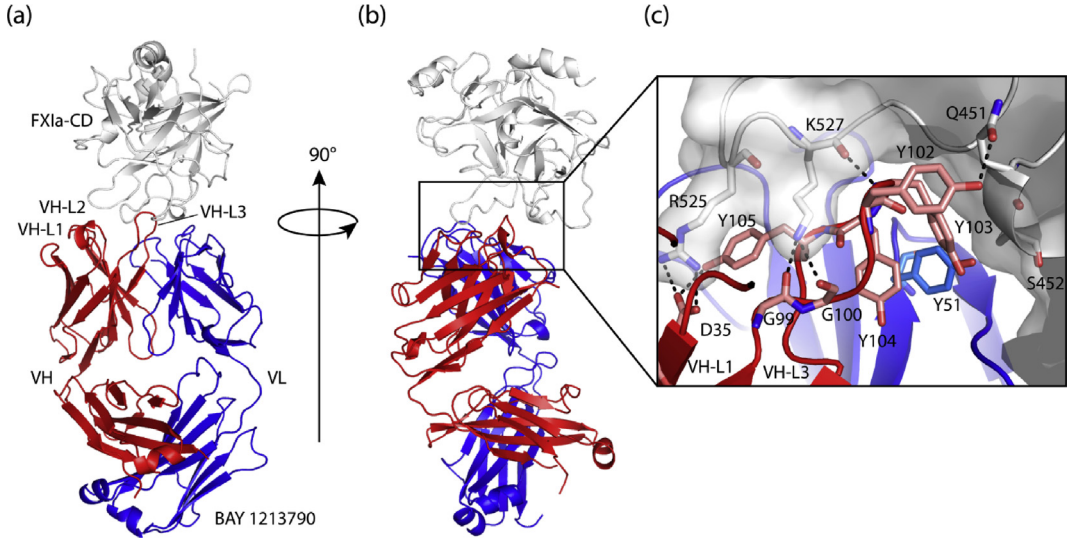

Fig. 3. Structural Arrangement of Human FXIa-CD and the Corresponding Fab Fragment of BAY 1213790. (a and b) Overall structural arrangement of FXIa-CD (gray) in complex with BAY 1213790-Fab. The heavy chain (VH) and light chain (VL) of BAY 1213790-Fab are shown in red and blue, respectively. (b) is rotated 90° clockwise compared with (a). (c) Interaction pattern of the VH CDR1 and CDR1 loops of BAY 1213790-Fab: Hydrogen bonds between amino acids are drawn as black dotted lines. Only side chains of amino acids involved in intra- and intermolecular contacts between BAY 1213790 and FXIa-CD are displayed as stick model.

BAY 1213790 to FXIa-CD. Mutational studies would allow a more quantitative statement.

The contribution of VL CDRs to binding was limited; the only interactions observed derived from CDR3 (Phe96 forming hydrophobic interactions with Leu524, and Asn94 forming an H-bond with Lys523 of FXIa-CD (Fig. S3)) and CDR1 (Tyr34 π-stacking to Lys523 of FXIa). An Asn94Asp mutation in CDR3 increased the affinity of the antibody for FXIa tenfold, which most likely resulted in the formation of a salt bridge between the Asp94 of CDR3 and Lys523 of FXIa, stabilizing the complex.

Structural rearrangements occurred on binding of BAY 1213790-Fab to FXIa-CD

The epitope recognized by BAY 1213790-Fab was very close to the FXIa-CD active site but there was little or no overlap (Fig. 4a); all amino acids contributing to the epitope are listed in Table S2. In comparison, the epitope recognized by the active site inhibitor PN2KPI (Kunitz protease inhibitor domain of protease nexin 2 [61]) was completely different to that recognized by BAY 1213790-Fab (Fig. 4b). This observation is also true for other small molecule inhibitors [31−36].

Binding of BAY 1213790-Fab to FXIa-CD resulted in various structural rearrangements. Most strikingly, there was a large reorientation of the loop from Arg522 to Lys527 (Arg144 to Lys149 using chymotrypsin nomenclature) forming one wall of the P2′ site. In zymogen FXI, this loop was completely disordered and not modeled into the electron density at all (Fig. 5a). In apo- or complex structures with active site inhibitors, this loop forms part of the P2′ pocket of FXIa-CD near the N-terminal amino acids of FXIa-CD, stabilizing the formation of the oxyanion hole (Fig. 5b). In the structure presented here, the loop opens by approximately 7 Å, allowing penetration of Arg525 between CDR2 and CDR3 of VH of BAY 1213790-Fab (Fig. 5c). In addition, one part of a loop forming one wall of the P1 pocket (Ala570 to Gly573) was shifted slightly inward, preventing S1 substrate residues from binding to FXIa-CD (Fig. 5d).

In parallel with the X-ray crystallography approach, the binding epitope of BAY 1213790-Fab was also determined by amide hydrogen/deuterium (H/D) exchange (Fig. 6d). The two methods elucidated almost identical epitopes (Fig. 6a and b).

Strongest protection against exchange of hydrogen to deuterium can be observed in the region covering amino acids Arg522 to Gln533 (average of >30% deuteration level difference) corresponding to the reorientated loop seen in the X-ray structure. A second region protected against H/D exchange with an average deuteration level difference of >10% ranges from amino acids Val444 Lys455. This second region constitutes the part of the binding epitope interacting with CDR loop 3 of the VH of BAY 1213790-Fab further supporting our hypothesis that CDR loop 3 contributes most to binding of BAY 1213790 to FXIa-CD. Weak protection but still covered by BAY 1213790-Fab is observed in a

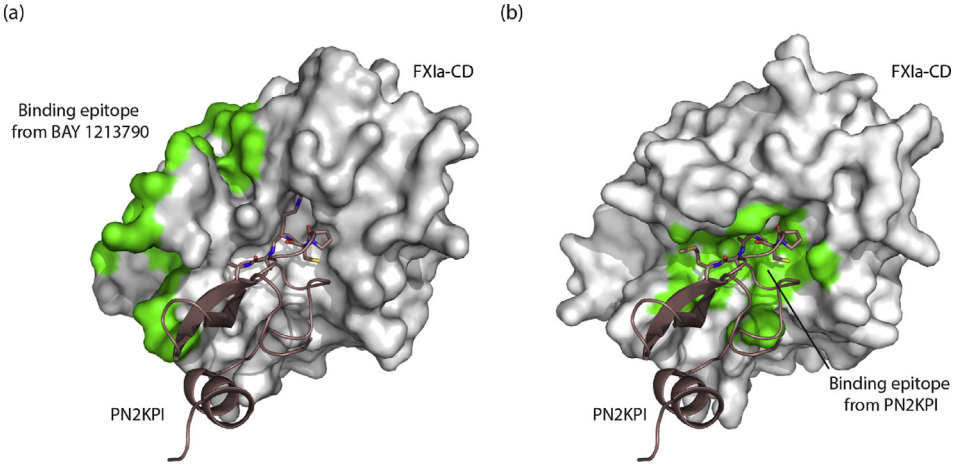

Fig. 4. Binding Epitope of FXIa-CD with BAY 1213790-Fab compared to Binding Epitope of FXIa-CD with PN2KPI [61]. (a) The surface of FXIa-CD (gray) as derived from our X-ray structure in complex with BAY 1213790-Fab. BAY 1213790-Fab has been removed for clarity. The epitope recognized by BAY 1213790-Fab is highlighted in green. To highlight the position of the active site of FXIa-CD the superimposed structure of the active site inhibitor PN2KPI (PDBcode 1ZJD) is shown as a brown ribbon. (b) The surface of FXIa-CD (gray) and active site inhibitor PN2KPI (brown) from 1ZJD. The epitope recognized by PN2KPI is highlighted in green. The orientation of (b) is similar as shown in (a).Both epitopes recognized by BAY 1213790 and PN2KPI were calculated using a 4 Å sphere around BAY 1213790 and PN2KPI and are highlighted in green, respectively.

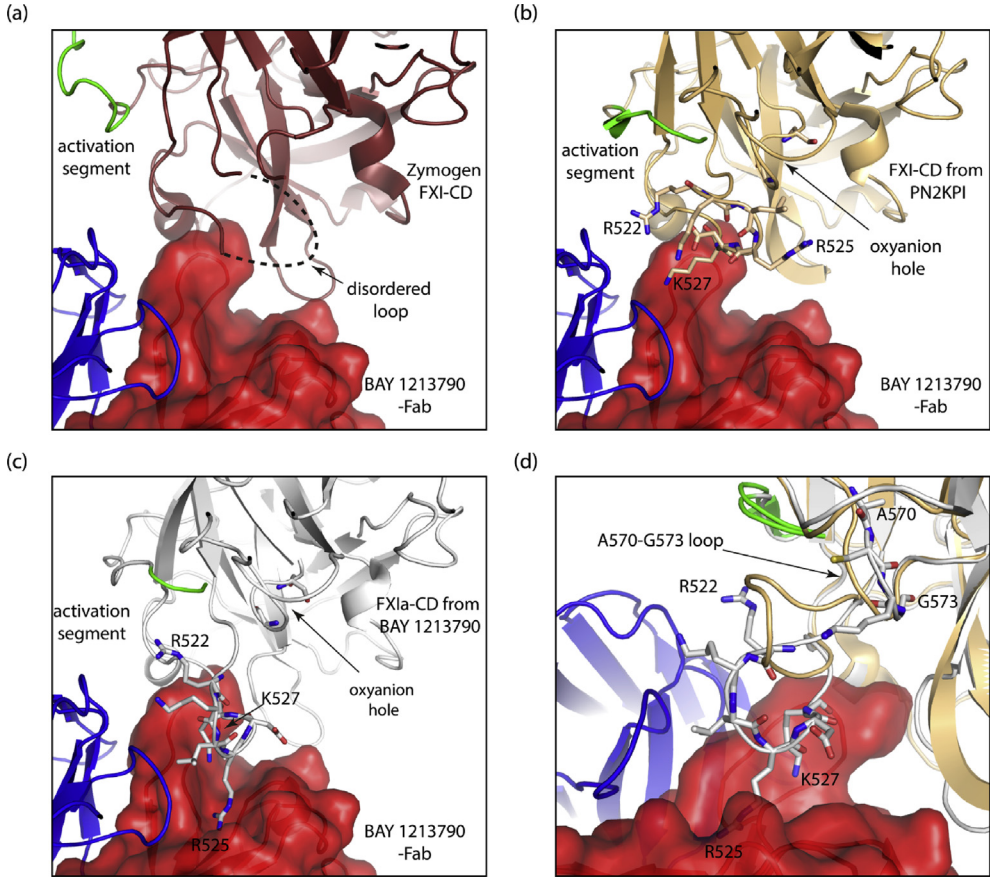

Fig. 5. Conformational Changes on Binding of BAY 1213790-Fab to FXIa-CD. FXIa-CD in complex with BAY 1213790-Fab, zymogen FXI (2F83), and FXIa in complex with PN2KPI (1ZJD) were superimposed based on their catalytic domains. In each figure BAY 1213780-Fab is displayed (VL shown as red surface, VH as blue cartoon) to emphasize the different structural rearrangements. (a) FXI zymogen (from 2F83, maroon color) shown together with BAY 1213790-Fab. The activation segment (green) is still bound to the A4 domain (not shown) and is not folded into FXI-CD. The disordered loop region Arg522 to Lys527 of zymogen FXI is highlighted as dotted lines. (b) X-ray of FXIa-CD in complex with PN2KPI (1ZJD, light orange) shown together with BAY 1213790-Fab. In this structure, the activation segment is folded towards the active site and the loop ranging from Arg522 to Lys527 (amino acids are displayed as sticks) is folded properly to form one border of the P2′ site of active FXIa. This loop also stabilizes the formation of the oxyanion hole important for activation of FXI. (c) X-ray of FXIa-CD (gray) in complex with BAY 1213790-Fab. On binding of BAY 1213790-Fab the Arg522 to Lys527 loop (shown as sticks) is folded by ~7 Å toward a cleft formed by VL-CDR2 and VL-CDR3 of BAY 1213790-Fab allowing side chain of Arg525 penetrate deepest into of BAY 1213790-Fab. (d) Superimposition of the FXIa-CD derived from our X-ray structure (gray) with FXIa-CD X-ray of PN2KPI complex (light orange). The orientation of this view is turned by a few degrees anticlockwise compared to (a–c). Here, only the amino acids from the Arg522 to Lys527 loop and the Ala570 to Gly573 loop from our structure are displayed as sticks, respectively. In the PN2KP1 X-ray structure the Ala570 to Gly573 loop forms one wall of the S1 pocket whereas in our FXIa-CD complex with BAY 1213790 this loop is shifted slightly inward. This shift blocks the active site for binding of substrate molecules.

range from amino acids Thr408 to Gln424 including Arg413 (average of 5–10% deuteration level difference).

BAY 1213790 inhibited FXIa via a novel allosteric mechanism

The X-ray structure of BAY 1213790-Fab in complex with FXIa-CD revealed reorientation of subsites important for substrate binding, indicating a novel allosteric mechanism of FXIa inhibition. Analyzing the biochemical data (Fig. 2) according to the Lineweaver–Burk equation of enzyme kinetics confirmed that BAY 1213790 binds in a competitive allosteric mode to FXIa (Fig. 6c).

FXIa-CD and the catalytic domains of other serine proteases did not overlap with the BAY 1213790 binding epitope

A sequence comparison of the novel epitope, as well as a structural superimposition of FXIa-CD and

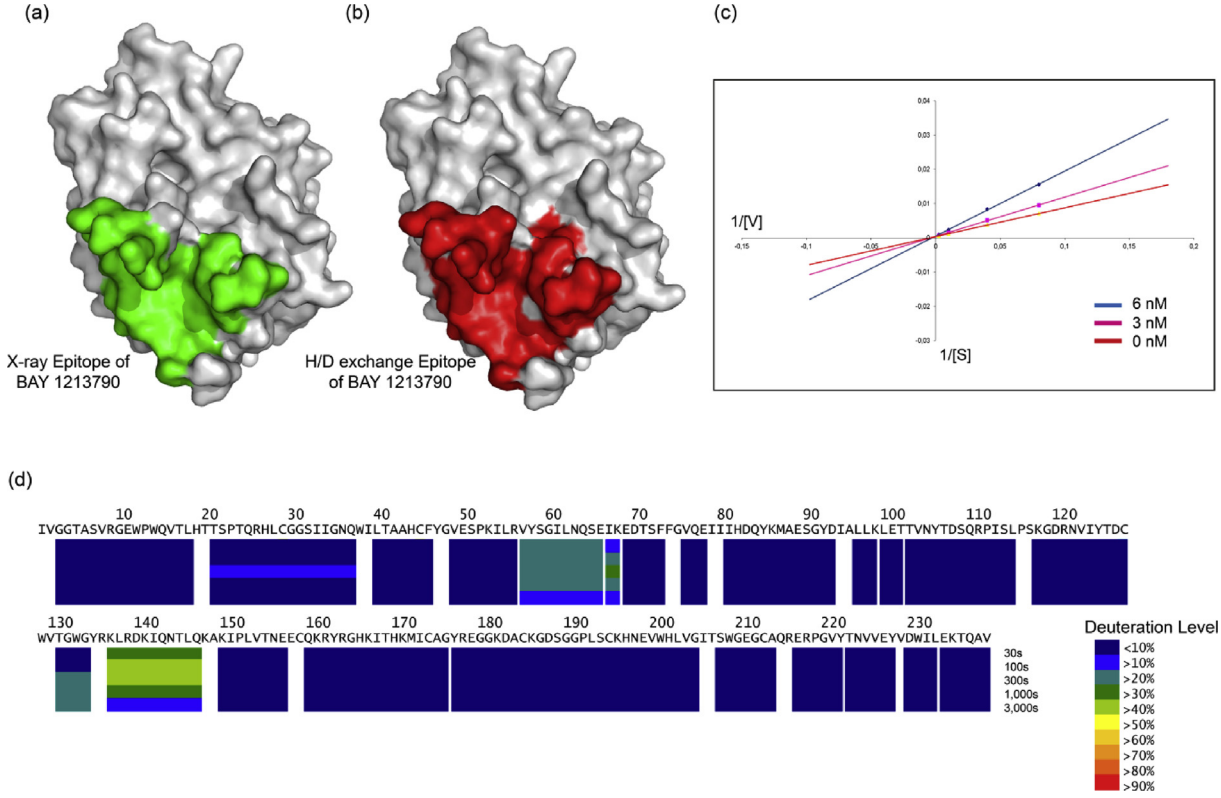

Fig. 6. Binding Epitope and Characterization of the Mode of Binding of BAY 1213790. (a) and (b) binding epitope determined by X-ray (a) and H/D exchange (b) of FXIa-CD in complex with BAY 1213790-Fab. The X-ray epitope is colored green; the H/D exchange epitope is colored red. The X-ray binding epitope was calculated using a 4 Å sphere around BAY 1213790-Fab. The H/D exchange epitope was taken from the results depicted in (d). (c) Characterization of the binding mode of BAY 1213790 using the Lineweaver–Burk plot. V, reaction velocity; [S], substrate concentrations of 400 nM, 100 nM, 25 nM, and 12.5 nM. (d) Difference in deuteration levels for each segment of FXIa in the presence or absence of BAY 1213790-Fab at pH 7.0 at 23 °C. Each block represents an analyzed peptide and contains five time points: 30, 100, 300, 1,000, and 3000 s. Dark blue indicates that there is no protection on BAY 1213790-Fab binding. Other colors indicate more or less deuteration in the presence of BAY 1213790-Fab, as shown in the right insert. The numbers above the amino acid sequence starts at 1 and are consecutively; they do not represent the FXIa-CD numbering. The two most protected region range from Arg522 to Gln533 (numbers 136–147, average of >30% deuteration level difference) and from Val444 to Lys455 (numbers 57–68, average of >10% deuteration level difference). Weak protection is observed for amino acids Thr408 to Gln424 (numbers 21 to 37, average of 5–10% deuteration level difference).

the catalytic domains of FXa, FVIIa, tissue plasminogen activator, plasma kallikrein, trypsin, and chymotrypsin derived from in-house or publicly available X-ray structures, supported the observation that BAY 1213790 did not inhibit any protease in a broad protease panel. Amino acids constituting the novel epitope were not conserved in other serine proteases (Fig. 7, amino acids constituting the binding epitope are highlighted in black). Inspection of the three amino acid regions constituting the binding epitope for BAY 1213790-FAB revealed that only three amino acids are partly conserved between FXIa and one or the other protease. K523 (position 173 in Fig. 7) is conserved in Trypsin, R525 (position 175 in Fig. 7) is conserved in FVIIa, and H414 (position 51 in Fig. 7) is conserved in Chymotrypsin, Trypsin, and Plasmin. The low degree of sequence conservation between the different proteases to FXIa for the newly identified binding epitope is therefore totally in line with the experimental observed cross-selectivity.

BAY 1213790–Inhibited Intrinsic Pathway-Mediated Activation of the Coagulation Cascade in Functional Assays

The ability of BAY 1213790 to inhibit intrinsic pathway-mediated activation of the coagulation cascade was subsequently tested in functional assays.

Global Coagulation Assays in Human Plasma

The activated partial thromboplastin time (aPTT) is a clotting time assay sensitive to inhibition of intrinsic

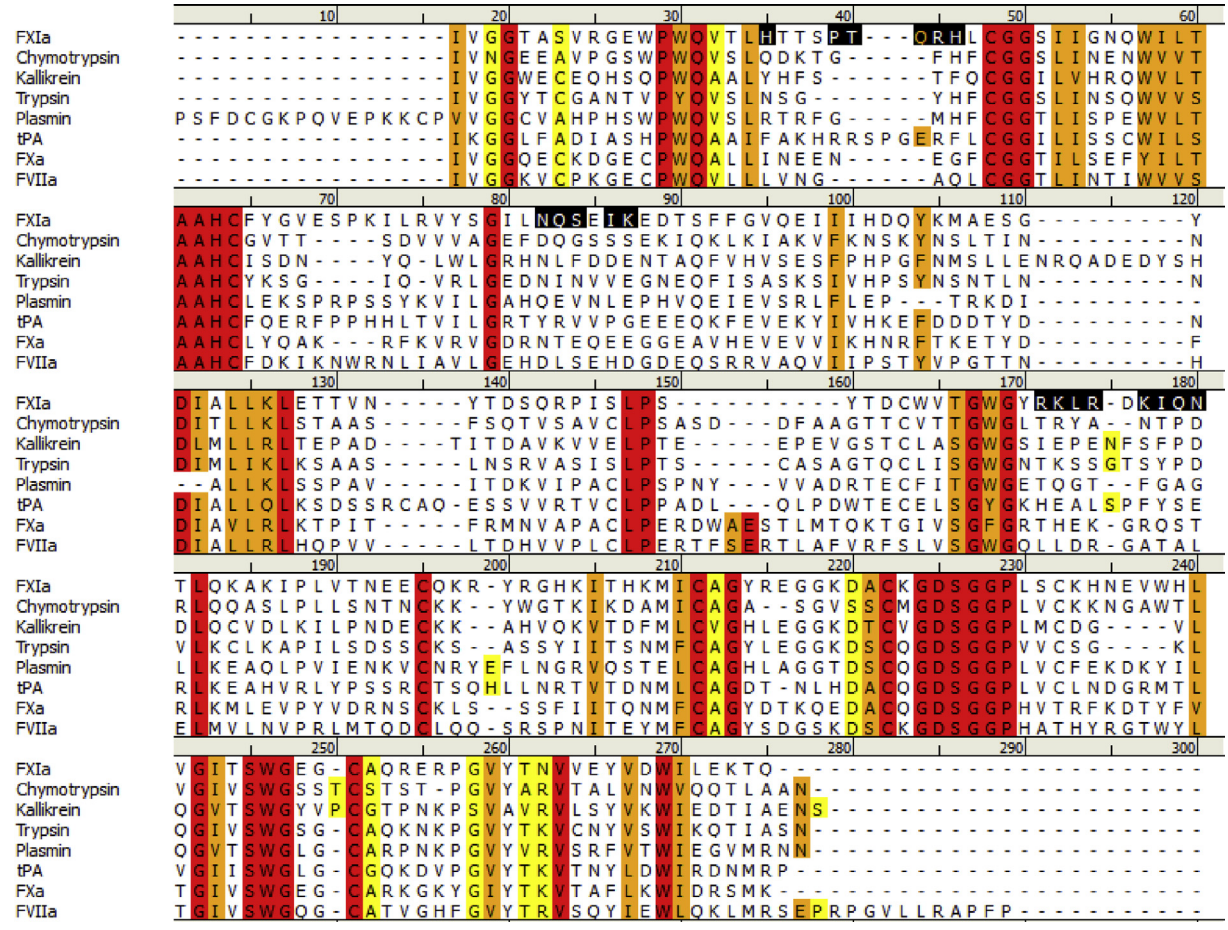

Fig. 7. Sequence Alignment of the Catalytic Domain of Selected Serine Proteases. Sequences of FXIa, FXa, FVIIa, and tissue plasminogen activator (tPA) were extracted from in-house X-ray structures. Sequences from plasmin, kallikrein, trypsin, and chymotrypsin were extracted from publicly available X-ray structures (plasmin 1V2O; trypsin 5UGD; kallikrein 1XX9; chymotrypsin 4CHA). Identical amino acids are highlighted in red; amino acids with strong and weak similarity are highlighted in orange and yellow, respectively. Nonconserved amino acids have a white background. The FIXa-CD epitope is highlighted in black.

coagulation factors such as FXIa. At a concentration of 20 nM (n = 16), BAY 1213790 was associated with a 1.5-fold prolongation of aPTT (Fig. 8a). BAY 1213790 did not prolong prothrombin time (which assesses activation of the extrinsic coagulation pathway) at any of the concentrations tested (data not shown).

Thrombin generation assay in human plasma

Thrombin generation is triggered by both the intrinsic and extrinsic pathways. BAY 1213790 inhibited thrombin generation (triggered with phospholipids at a very low concentration of tissue factor) in a concentration-dependent manner (Figs. 8b and S4). Endogenous thrombin potential and peak thrombin concentration were inhibited at an IC_{50} of 0.12 ± 0.03 μM and 0.035 ± 0.01 μM (n = 5), respectively (Fig. S4). BAY 1213790 was associated with a twofold greater prolongation (vs control) of the time to the peak of thrombin generation and thrombin generation lag time at concentrations of 0.27 ± 0.02 μM and 0.88 ± 0.09 μM, respectively (n = 5) (Fig. S4).

Clotting time measured using nonactivated rotational thromboelastometry

Thromboelastometry measures the viscoelastic properties of citrate-anticoagulated blood under low shear conditions that resemble the rheologic properties of slow-moving venous flow. BAY 1213790 prolonged the clotting time of human whole blood in a concentration-dependent manner (Fig. 8c). The concentration of BAY 1213790 required to double the clotting time was 0.14 μM.

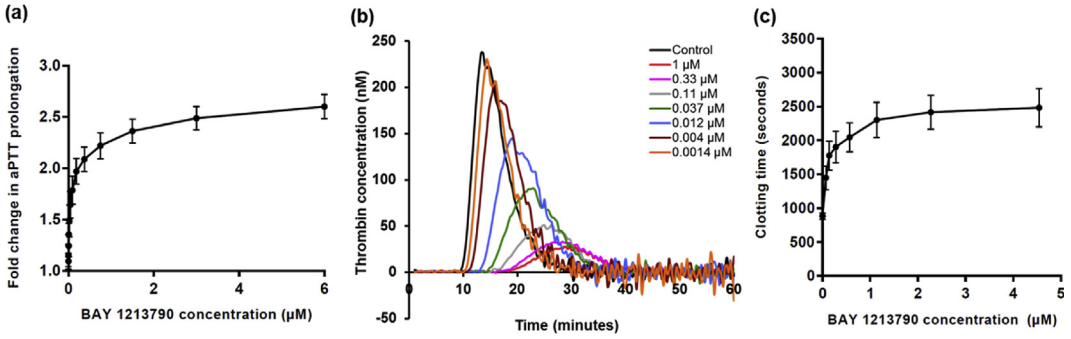

Fig. 8. Effect of BAY 1213790 on Coagulation Assays in Human Plasma. (a) Effect of BAY 1213790 on aPTT in human plasma. Data shown are means ± standard deviation (n = 16). (b) Effect of BAY 1213790 on thrombin generation in human plasma. A representative set of curves is shown. (c) Effect of BAY 1213790 on clotting time in human whole blood, measured by nonactivated rotational thromboelastometry. Data shown are means ± standard error of the mean (n = 5).

Discussion

FXI has emerged as a promising target for novel anticoagulants that have the potential to reduce thrombosis risk while minimizing the risk of bleeding [2,30]. This study describes the generation of BAY 1213790, a monoclonal antibody directed against human FXIa. It also reports investigation of the crystal structure of BAY 1213790-Fab in complex with FXIa-CD, and the anticoagulant effects of BAY 1213790.

A medium-resolution cocrystal structure of BAY 1213790-Fab in complex with FXIa-CD was analyzed. Results of this analysis demonstrated that the CDR3 of the heavy chain of BAY 1213790 and, to a lesser extent, the CDR1 of the light chain, were the main drivers of binding to FXIa. The epitope on FXIa recognized by BAY 1213790 was different to that recognized by PN2KPI, which binds the active cleft of FXIa [61]. Small-molecule inhibitors reported in the literature [29,31−39,62], as well as those discovered using in-house X-ray structures (data not shown), also recognize epitopes that are different to the epitope described herein for BAY 1213790-Fab. BAY 1213790 bound to a region adjacent to the active site of FXIa, leading to substantial structural rearrangements. This suggested an allosteric mechanism of inhibition of FXIa, as confirmed by biochemical data. More specifically, remodeling of the P2′ active site and subsequent decrease in binding to substrate residues of the P1 pocket might be the driver for the allosteric mechanism of BAY 1213790. These observations explain the ability of BAY 1213790 to prevent cleavage of the natural substrate FIX by FXIa and thus its anticoagulant effects. Furthermore, on activation of FXI zymogen to FXIa, disordered regions in the FXI catalytic domain became ordered (mainly parts of the P2′ pocket). This structural ordering explains why BAY 1213790 only inhibits FXIa and not the FXI zymogen.

Among the coagulation proteases, FXI has a unique, homodimeric structure [4,42]. The dimeric structure of FXI is likely to be important for at least some aspects of its function. It is well accepted that, via a transactivating mechanism, binding of FXIIa or thrombin to one FXI subunit leads to the activation of the other monomer [55]. Therefore, the common understanding is that this transactivation is bidirectional. In 1977, Bouma and Griffin proposed the existence of a half-activated form of FXIa, in which only one subunit is cleaved and therefore already activated [63,64]. This hypothesis was further supported by new data reporting that FXI activation by FXIIa or thrombin leads to an intermediate in which only one monomeric subunit of the dimer is cleaved [64]. This intermediate, termed 1/2-FXIa, exhibits proteolytic activity: it is able to cleave its natural substrate FIX and promotes clot formation in plasma [64]. The authors postulate that both FXIIa and thrombin slowly activate FXI to fully activated FXIa, and that 1/2-FXIa may be a major form of active FXI in plasma [64]. With these data showing that BAY 1213790 binds to a loop region only accessible in the activated form of FXI, it may be that the antibody BAY 1213790 binds to one half of the activated dimer. This conclusion is based on indirect evidence; therefore, further studies are needed to clarify these findings in more detail.

The specificity of BAY 1213790 for FXIa over FXI was also demonstrated by enzyme-linked immunosorbent assay (ELISA) measurements, which showed potent binding to FXIa, whereas binding to the FXI zymogen was not detected. This specificity might be a desirable property because theoretically, BAY 1213790 would only act during active coagulation, after generation of FXIa. The zymogen FXI would not be depleted by BAY 1213790 and dosing would be independent of synthesis of new FXI.

Allosteric binding sites of proteases are much less likely to be conserved than orthosteric sites, which means that allosteric inhibitors have potentially

greater specificity than orthosteric inhibitors. Moreover, the efficacy of an allosteric inhibitor is dependent on the efficiency of energy transmission from the allosteric site to the active site [62], which allows the anticoagulant effect to be modulated as a function of dose [62]. The majority of small-molecule inhibitors of FXI/XIa are orthosteric inhibitors [31–36,62]; however, some allosteric FXIa inhibitors have been reported [37–39].

Although monoclonal antibody inhibitors of FXI/FXIa have been developed, none have been reported to be allosteric inhibitors. The monoclonal antibody 14E11 binds to FXI apple domain A2 and inhibits its activation by FXIIa but does not affect FXIa activation of FIX [18], and O1A6 specifically recognizes the A3 apple domain of FXI heavy chain [26]. The monoclonal antibodies αFXI-175 and αFXI-203 bind the A4 and A2 domains, respectively [28]. In contrast, XI-5108 binds to the catalytic domain, but an allosteric mechanism was not reported; rather, XI-5108 physically prevents the binding of substrates to FXIa [27]. Recently, an X-ray of the first anti-FXIa monoclonal antibody (DEF) was published [29], demonstrating that DEF binds in a competitive manner, occupying P1, P2, P3, and P2′ of FXIa. There is only little overlap at the borders between the epitopes recognized by DEF and BAY 1213790, respectively (Fig. S5) namely parts of the reoriented loop from Arg522 to Lys527 and few amino acids from a beta-sheet stretch from Pro410 to His414. The finding that both FABs occupy different epitopes on FXIa-CD is supported by the fact that binding of DEF to FXIa is not disrupted by BAY 1213790 [65]. The newly identified epitope recognized by BAY 1213790 is so far not reported in the literature as a known binding site on FXI/FXIa.

Suboptimal binding specificity has generally been a drawback for small-molecule inhibitors and this makes monoclonal antibodies, with their inherent target specificity, an attractive strategy. Consistent with this, BAY 1213790 was highly specific for human FXIa, and binding to other serine proteases was not detected. This is important to minimize the risk of unintended effects on the clotting cascade, especially an increase in bleeding. The lack of binding to kallikrein, which has an amino acid sequence approximately 58% homologous to that of FXI, is particularly advantageous; in contrast, the IC_{50} for the small-molecule inhibitor BMS-262084 has been reported as 2.8 nM against FXIa compared with 110 nM against plasma kallikrein [66]. Although plasma kallikrein converts FXII to FXIIa, which in turn activates FXI, it also cleaves high-molecular-weight kininogen to release bradykinin. This has wide-ranging effects on inflammation, vascular function, blood pressure regulation, and nociceptive responses [67].

The present *in vitro* studies demonstrated that binding of BAY 1213790 to FXIa leads to allosteric inhibition of FXIa activity. Functional assays showed that this inhibition of FXIa by BAY 1213790 translates into anticoagulant activity. Specifically, in human plasma, BAY 1213790 prolonged aPTT, a clotting time assay sensitive to inhibition of intrinsic coagulation factors such as FXIa. BAY 1213790 also inhibited thrombin generation in human plasma and prolonged the clotting time of human whole blood in a concentration-dependent manner. In conclusion, as therapeutic agents, antibodies have advantages over ASOs and most small molecules, including greater specificity and a rapid onset of action [68]. The offset of action of antibodies is slow (ranging from days to weeks), which has advantages in terms of dosing frequency, but may be a disadvantage in some circumstances, for example, during some types of surgery in which there is an increased risk of bleeding. Notwithstanding, the present data describing the structural basis for interaction between BAY 1213790 and FXIa suggest that this anti-FXIa monoclonal antibody inhibits FXIa via a novel allosteric inhibition mechanism with high specificity, and as such, may be a promising antithrombotic compound.

Material and Methods

Identification and generation of BAY 1213790

Phage library selection

The general library selection method has been described previously [60]. Briefly, proteins for the isolation of human antibodies against FXIa (Table S1) were biotinylated using an approximately twofold molar excess of biotin-LC-NHS (Pierce) according to the manufacturer's instructions and desalted using Zeba desalting columns (Pierce). Biotinylated proteins (Table S1) were then captured on M280 streptavidin-coated magnetic beads (Invitrogen) before incubation with the phage library. Selection against the biotinylated proteins of interest (Table S1) was made using the FAB-310 library (Dyax Corp). This human Fab antibody library combines natural and synthetic diversity.

Tables S2–S6 summarize the different strategies that were used to select antibodies covering multiple epitopes. Briefly, the Fab antibody library was precipitated and incubated in blocking buffer at room temperature for 30 min. M280 streptavidin-coated magnetic beads (Dynabeads) were washed with phosphate-buffered saline (PBS) plus Tween 20 (PBST; Sigma-Aldrich) and mixed with biotinylated protein (Table S1). The mixtures were incubated overnight at 4 °C, washed in PBST, and resuspended in blocking buffer, from which the beads were then recovered.

As indicated in Tables S2–S6, five sequential depletion steps were carried out by adding the blocked library (described earlier) to blocked Dynabeads coated with biotinylated kallikrein/pre-kallikrein (500 nM) or biotinylated human FXI (500 nM) and incubating at room temperature for 10 min while rotating. After collection of

the beads, the supernatant was mixed with blocked Dynabeads coated with the target protein (Tables S2–S6). After 30 min of incubation with rotation, the samples were washed with blocking buffer, then with PBST.

Half of the resuspended beads containing enriched phages were used to infect exponentially growing *Escherichia coli* TG1 (Stratagene) for preparation of new phage stocks used in the next selection round according to the strategies provided in Tables S2–S6. *E. coli* TG1-culture (6 mL) was infected with Dynabead/phage suspension (500 μL) for 30 min at 37 °C without shaking. Pelleted and resuspended cells were grown on 2X YT (yeast extract tryptone) agar plates containing 100 μg/mL ampicillin and 2% glucose overnight at 37 °C and used to inoculate 20 mL fresh liquid culture (optical density at 600 nm [OD_{600}]: 0.05). This was shaken for approximately 2 h at 37 °C until an OD_{600} of 0.5–0.8 was reached, then 5 mL was mixed with M13 helper phage M123K07 (Invitrogen) at a multiplicity of infection of approximately 20. After slow shaking for 30 min at 37 °C, 30 mL prewarmed 2X YT containing 100 μg/mL ampicillin and 20 μg/mL kanamycin (final concentrations) was added and the culture was shaken overnight at 30 °C. The supernatant was harvested and filtered (Steriflip 0.22 μM; Millipore). Subsequently, phages were precipitated and resuspended in blocking buffer (or cell panning buffer) for use in the next selection round.

Phage ELISA

Phage pools from each round of selection were analyzed for the enrichment of specific binding by ELISA on biotinylated target proteins. Briefly, aliquots from the glycerol stocks of phage-infected *E. coli* cells were plated on 2X YT agar (100 mg/mL ampicillin, 1% glucose). Single colonies were added to microtiter plate wells (medium 2X YT, 100 μg/mL ampicillin, 1% glucose) and shaken overnight at 37 °C. Phage expression was detected by adding overnight culture to fresh medium containing helper phage M123K07 (Invitrogen) and incubating at 200 rpm and 37 °C in microtiter plates until an OD_{600} of approximately 0.5 was reached.

ELISA plates precoated with streptavidin (Pierce) were coated overnight at 4 °C with 1 μg/mL biotinylated target protein, washed with PBST, and treated with blocking buffer. The plates were incubated for 1 h at room temperature with overnight phage cultures in blocking buffer. After PBST washes, the plates were incubated for 1 h at room temperature with horseradish peroxidase–conjugated anti-M13 antibody (GE Healthcare; 1:2500 diluted in PBST), then washed again. A color reaction was developed with 3,3′,5,5′-tetramethylbenzidine (TMB; Invitrogen) and stopped with H_2SO_4 (Merck). The colorimetric reaction was recorded at 450 nM in a plate reader (Tecan).

Genotypic characterization sequencing

Candidate Fabs displaying inhibitory activity in FXI and FXIa biochemical activity assays were submitted for genotypic characterization sequencing by a contract research organization (Qiagen N.V.), according to their protocols. Genotypic characterization sequencing was used to identify clones with unique sequences in their CDRs. Hits were recloned to generate full-length antibodies and selected for subsequent recombinant expression and purification. Validated candidates were considered for in-depth analysis.

Expression and quantification of BAY 1213790

Transient production of BAY 1213790 in suspension HEK293-6E cells was performed using methods described in detail elsewhere [69,70]. Briefly, TubeSpin Bioreactor 50 (TPP; 35 mL culture volume) or 96 half-deep well plates using sandwich covers (Enzyscreen System Duetz; 200 μL culture volume) were used for expression of BAY 1213790. To assess the predictivity of a high-throughput transfection system to a later upscale in expression, mini-prep-derived DNA was used for deep-well plate expression and midi-prep-derived DNA was used for expression in 35 mL TubeSpins. The cultures were cleared from the cells using centrifugation 5 days after transfection. Expression levels of BAY 1213790 were determined using protein A chromatography on an Agilent 1200 high-performance liquid chromatography system (POROS A/20, Applied Biosystems; 2.1 mm diameter × 30 mm length). The resulting peak was detected at an optical density of 280 nm, integrated and quantified using human immunoglobulin G1 (IgG1) as reference for calibration.

BAY 1213790–Fab generation and purification

The Fab portion of BAY 1213790 was generated by papain cleavage of the full-length IgG1. The IgG1 (20 mL at a concentration of 20 mg/mL) was incubated for 4 h at 37 °C with 30 mL of immobilized papain (Thermo Fisher Scientific). The reaction buffer contained 20 mM Na_3PO_4 (pH 7.0), 10 mM ethylenediaminetetraacetic acid (EDTA), and 20 mM cysteine hydrochloride. The solution was centrifuged for 10 min at 800 × *g* and the resulting supernatant was removed. For purification of the Fab, the supernatant was passed through a MabSelect SuRe column (GE Healthcare). The flow-through was analyzed by sodium dodecyl sulfate polyacrylamide gel electrophoresis (SDS-PAGE), and the fractions containing the Fab were pooled for further experiments.

Selectivity assays

The inhibitory potency and/or selectivity of BAY 1213790 was determined by the fluorescent detection of aminomethyl coumarin (AMC), released from fluorogenic peptidic protease substrates on protease-catalyzed cleavage. Coupled protease reactions are applied for assaying Factor VIIa using FVIIa, tissue factor, Factor X and Factor Xa substrate. Details of the serine protease enzymes and fluorogenic substrates used in these assays are given in Table S7.

All enzymes and substrates were diluted in buffer comprising Tris/HCl (50 mM, pH 7.4), NaCl (100 mM), $CaCl_2$ (5 mM), and bovine serum albumin (BSA; 0.1%). White 384-well microtiter plates (Greiner) containing 1 μL/well serial dilutions of test or reference compounds were incubated with 20 μL assay buffer, 20 μL enzyme dilution, and 20 μL substrate. When BAY 1213790 (22.05 mg/mL [145 μM] in PBS) was the test compound, it was diluted in assay buffer 1:4.8, and 20 μL was added to the test plate,

replacing the 20 μL assay buffer. After incubation for typically 30 min (linear reaction kinetics) at room temperature, fluorescence (excitation: 360 nm, emission: 465 nm) was measured in a microtiter plate fluorescence reader (e.g., Tecan Safire II). IC_{50} values were determined by plotting log test compound concentration against the percentage protease activity.

Biochemical characterization of BAY 1213790

ELISA

The binding affinity of BAY 1213790 to FXI and FXIa (Haematologic Technologies Inc.) was examined using ELISA. Black, 384-well Maxisorp microtiter plates (Nunc) were incubated overnight at 4 °C with the antigens, which were diluted to 1 μg/mL in ELISA coating buffer 1X (Candor Bioscience). The plates were washed with PBST and incubated for 1 h at room temperature with SmartBlock blocking buffer (Candor Bioscience). Plates were washed again with PBST and incubated for 1 h at room temperature with different concentrations of BAY 1213790 (starting at a concentration of 2×10^{-6} M, followed by 1:3 dilutions for 15 dilution steps; final volume 30 μL per well). After three PBST washes, bound BAY 1213790 was detected with anti-h-Fc-POD antibody (Sigma), which was diluted 1:10 000 in 10% blocking buffer (final volume 30 μL per well). Plates were then incubated for 1 h at room temperature. Following further PBST washes, a mixture of 1:1000 Amplex Red (Invitrogen; 10 mM stock solution in dimethyl sulfoxide) and 1:10 000 H_2O_2 (Merck; 30% stock solution) were added as the substrate, and the plates incubated for 20 min in the dark. The readout was analyzed using the Infinite F500 reader (Tecan) in fluorescence measurement mode: top reading; excitation, 535 nm; emission, 590 nm.

Data were analyzed using the GraphPad Prism software; binding activity of BAY 1213790 was calculated as EC_{50} values. All experiments were performed four times and data are given as mean ± standard error of the mean.

SPR affinity determination of FXIa and BAY 1213790

The binding affinity (KD value) of BAY 1213790 was determined by SPR using a Biacore T100 instrument (GE Healthcare) equipped with Series S Sensor Chips CM5 (GE Healthcare). Binding assays were conducted at 25 °C with assay buffer HBS-EP+ (10 mM HEPES [4-(2-hydroxyethyl)-1-piperazineethanesulfonic acid] pH 7.4, 150 mM NaCl, 0.05% polysorbate 20) supplemented with 1 mg/mL BSA and 0.05% NaN_3. BAY 1213790 was captured with an antihuman IgG1 capture antibody covalently immobilized to the chip surface via amine coupling chemistry. Reagents for amine coupling (1-ethyl-3-(3-dimethylaminopropyl)carbodiimide hydrochloride [EDC], N-hydroxysuccinimide [NHS] and ethanolamine-HCl, pH 8.5) were obtained from the Amine Coupling Kit (GE Healthcare). Anti-IgG1 capture antibody and immobilization buffer (10 mM sodium acetate, pH 5.0) were obtained from the Human Antibody Capture Kit (GE Healthcare). The sensor chip surface was activated with a freshly prepared solution of 0.2 M EDC and 0.05 M NHS passed over the chip surface for 420 s at a flow rate of 10 μL/min, followed by an injection of anti-IgG1 capture antibody (dissolved to 25 μg/mL in immobilization buffer) for 180 s at a flow rate of 5 μL/min. Excess activated groups were blocked with a 1 M solution of ethanolamine injected at a flow rate of 10 μL/min for 420 s.

Each experimental cycle consisted of a ligand capture step followed by injection of an analyte for kinetic interaction analyses and then injection of a regeneration solution. For capture of BAY 1213790 (ligand), the sample was diluted to 1 μg/mL with assay buffer HBS-EP+ (including 1 mg/mL BSA and 0.05% NaN_3) and injected for 20 s at a flow rate of 10 μL/min. Kinetic interaction analyses were performed with the monomeric catalytic domain of human FXIa (FXIa-CD) as the analyte. In all experiments that utilized FXIa-CD, the Cys500Ser mutant, amino acids 388−625 (Proteros Biostructures), was used. FXIa-CD was consecutively injected in a twofold dilution series from 100 nM to 0.78 nM (12.5 nM injection run in duplicate) over captured BAY 1213790 at a constant flow rate of 30 μL/min for 180 s; dissociation was monitored for 600 s. After each concentration of FXIa-CD, the chip surface was regenerated with glycine-HCl (pH 2.0, 30 μL/mL for 20 s) to remove FXIa-CD and BAY 1213790 before starting a new cycle.

The obtained sensorgrams were double-referenced, that is, using in-line reference cell correction followed by buffer (zero concentration) sample subtraction. The KD value was calculated based on the ratio of dissociation (kd) and association (ka) rate constants, which were obtained by globally fitting sensorgrams with a first order 1:1 Langmuir binding model.

Functional neutralization of FXIa

Human FXIa (final concentration, 10 nM) in buffer (50 mM Tris/HCl, 100 mM NaCl, 5 mM $CaCl_2$ and 0.1% BSA) was added to black low-volume 384-well microtiter plates (Greiner) at a final volume of 5 μL per well. Plates were centrifuged for 1 min at 500 × *g*. Various concentrations of BAY 1213790 (starting at a concentration of 6.2×10^{-8} M, followed by 1:2 dilutions for 11 dilution steps) were added to the plates at 5 μL/well and the plates were then centrifuged for 1 min at 500 × *g*. Plates were incubated for 1 h at 37 °C. FXIa activity and the function-blocking activity of BAY 1213790, respectively, were measured by the cleavage of a FXIa-specific, fluorogenically labeled substrate (Bachem) added to a final concentration of 25 μM. The readout was analyzed using the Infinite F500 reader (Tecan) in fluorescence measurement mode (top reading; excitation, 360 nm; emission, 465 nm) and in kinetic mode (13 cycles, 5-min sampling interval).

Data were analyzed using GraphPad Prism software. All experiments were performed four times, and data are given as mean ± standard error of the mean.

Biochemical FXIa neutralization assay

A plasma-based assay was used to test BAY 1213790 inhibition of FXIa activation of the natural substrate FIX. Human citrated plasma (Harlan Laboratories) was diluted in buffer (50 mM Tris/HCl, 100 mM NaCl, pH 7.4) to a final concentration of 30%. To avoid nonspecific cleavage of the fluorogenic FIXa substrate (SpectroFluor FIXa 299F;

American Diagnostica), the thrombin inhibitor Melagatran (1 μM, final concentration) and phospholipids (9%, final concentration) were added to the reaction mixture. Various concentrations of BAY 1213790 (starting at a concentration of 3.3×10^{-7} M, followed by 1:2 dilutions for 11 dilution steps) were diluted in the plasma/buffer mixture and incubated for 30 min at room temperature. Intrinsic coagulation was induced by addition of insoluble aluminum silicate kaolin (Acros Organics) at a final concentration of 12 μg/mL and $CaCl_2$ (12 mM, final concentration). The activity of FIXa, generated from the conversion of FIX by FXIa, was measured by adding the fluorogenic substrate 299F (140 μM, final concentration) and monitoring fluorescence continuously at 360/465 nm using a SpectraFluor Plus Reader (Tecan). Data were analyzed using GraphPad Prism software. All experiments were performed four times, and data are given as mean ± standard error of the mean.

Structure of the FXIa–BAY 1213790-Fab complex

Complex formation and crystallization

FXIa Cys500Ser (amino acids 388–625) was purchased from Proteros Biostructures. Purified BAY 1213790-Fab was mixed in a 1:1 ratio with FXIa Cys500Ser and stored for 18 h on ice. The complex solution was loaded on a Superdex 200 HR 16/60 column and was further concentrated to 20 mg/mL in 20 mM Tris/HCl at pH 7.5 and 75 mM NaCl. Crystals of the protein complex comprising BAY 1213790-Fab and FXIa Cys500Ser were grown at 20 °C using the sitting-drop method and crystallized by mixing equal volumes of protein complex solution and well solution (100 mM Tris pH 8.25, 0.05% PEG 20 000 and 2.4 M $(NH)_4SO_4$ as precipitant). A rosette-like crystal appeared after approximately 5 days.

Data collection and processing

The crystal was flash-frozen in liquid nitrogen without use of cryobuffer. Crystal data were collected at beamline BL14.1, BESSY synchrotron (Berlin) on a MarCCD X-ray detector. Data were indexed and integrated with XDS [71], prepared for scaling with POINTLESS [72] and scaled with SCALA [73].

Structure determination and refinement

The complex structure of FXIa and the monoclonal antibody BAY 1213790-Fab was solved by molecular replacement in multiple steps. First, the H-chain was located using BALBES [74], with a search model based on protein database (PDB) entry 3GJE. Then, FXIa Cys500Ser was added using the program MOLREP [75] with an internal FXIa crystal structure as the search model. Initial refinement with REFMAC5.5 [76] resulted in R1 = 39.4% and R_{free} = 44.1%. Finally, the H-chain was located using the L-chain of PDB entry 3IDX as the search model and fixed coordinates of the initially refined H-chain and FXIa Cys500Ser solution. Iterative rounds of model building with *Coot* [77] and maximum likelihood refinement using REFMAC5.5 completed the model. Data set and refinement statistics are summarized in Table S1. Figures were generated using Pymol [78].

BAY 1213790 binding epitope

X-ray crystallography

The binding epitope on FXIa recognized by BAY 1213790-Fab was determined using the program AREAIMOL (CCP4 package) [79]. The buried surface was analyzed and residues showing an area difference when calculated with bound and without bound BAY 1213790-Fab were assumed to constitute the binding epitope of FXIa.

H/D-exchange mass spectrometry-based epitope mapping

H/D-exchange mass spectrometry–based epitope mapping was performed by ExSAR (ExSAR Corporation). The interactions of FXIa Cys500Ser (amino acids 388–625; Proteros Biostructures) and purified BAY 1213790-Fab were analyzed by methods described previously [80]. Briefly, for the exchange experiment 0.52 mg/mL (19.3 μM) of FXIa Cys500Ser and 10.0 μL of 0–38.6 μM of BAY 1213790-Fab were mixed with 10.0 μL of PBS in D2O, pH 7.0, resulting in final concentrations of FXIa Cys500Ser of 0.26 mg/mL (9.63 μM) and of the BAY 1213790 Fab of 0.0–19.3 μM. This reaction mixture was incubated for 300 s at 23 °C. Afterwards, 20 μL of this reaction mixture was mixed with 30 μL of 2 M Urea, 1 M TCEP, pH 3.0 and 45 μL of the mixture was injected into the ExSAR system (+ C18 + pepsin). The quenched solution was loaded onto a reversed-phase trap column and desalted with 0.05% TFA in H2O at 200 μL/min for 3 min. The reaction was separated by a C18 column with a linear gradient of 13%–35% in 95% acetonitrile, 5% H2O, 0.0025% TFA) over a time period of in 23 min. Resulting fractions were analyzed by mass spectrometry. Differences in the deuteration level of more than 10% were taken to indicate a strong protection by the Fab of the corresponding antigen. Values between 5% and 10% were taken to indicate weak binding; those below 5% were taken to indicate no protection at all.

Anticoagulant effects of BAY 1213790

Global coagulation assays

Pooled human citrated plasma (Octaplas LG, Octapharma) was incubated with increasing concentrations (from 1.46 nM to 6 μM) of test compounds for 3 min at 37 °C and for a further 3 min with aPTT reagent (C.K. Prest 5, Diagnostica Stago) to initiate the intrinsic coagulation pathway. Coagulation was started by recalcifying the sample with 0.025 M prewarmed $CaCl_2$ solution. An automated coagulometer (AMAX 200, Trinity Biotech) mixed the plasma at 37 °C and mechanically recorded the time to clotting. The mean (±SEM) concentration of BAY 1213790 that prolonged aPTT by a factor of 1.5 (EC_{150}) was calculated from six repeated experiments. For the measurement of prothrombin time, thromboplastin (RecombiPlasTin; Instrumentation Laboratory) was added to initiate the extrinsic coagulation pathway.

Thrombin generation assay

Thrombin activity was monitored in clotting plasma (pooled human citrated plasma, Octaplas LG,

Octapharma) through continuous measurement of the fluorescent split products of the substrate I-1140 (Z−Gly−Gly−Arg−AMC, Bachem) [81]. The reaction was performed in 20 mM HEPES, 60 mg/mL BSA, 102 mM $CaCl_2$ at pH 7.5, and 37 °C. To start the reaction, 4 μM phospholipids (Rossix) and 0.1 pM tissue factor were added. Measurements were carried out in a Thermo Electron Fluorometer (Fluoroskan Ascent) equipped with a 390/460 nm filter set and a dispenser. All experimental steps were conducted according to the manufacturer's instructions (Thrombinoscope). Thrombograms (thrombin concentration vs time) were calculated using Thrombinoscope software, and from these, the following parameters were calculated: lag time (time taken for thrombin generation to begin); time to peak (time taken to reach peak thrombin concentration); maximum concentration of thrombin; and endogenous thrombin potential, which is the area under the curve of the thrombogram. Data are presented as mean ± standard error of the mean.

Nonactivated rotational thromboelastometry

Human blood was obtained from healthy volunteers who had not received medication in the previous 10 days. Written informed consent was obtained from all volunteers. All experiments were carried out in accordance with local ethical committee requirements. Human blood was collected by antecubital venipuncture using a 20G Multifly set (Sarstedt) into plastic tubes (Sarstedt 9 NC/10 mL monovettes) containing sodium citrate 3.2% (1/10) and preincubated at 37 °C on a shaker. A total of 20 μL $CaCl_2$ (0.2 M) was mixed with 20 μL antibody or solvent in a cuvette, followed by the addition of 300 μL blood. Measurements were performed using the ROTEM thromboelastography system (Pentapharm GmBH). Clotting time was defined as the period from the start of the analysis until the recognizable start of clot formation. Data are presented as mean ± standard error of the mean.

Accession Number

Coordinates and structure factors for FXIa in complex with BAY 1213790 have been deposited in the PDB with accession number 6HHC.

Acknowledgments

Medical writing support was provided by Emma Bolton DPhil of Oxford PharmaGenesis, Oxford, UK, funded by Bayer AG. The authors thank Axel Harrenga (Bayer AG) for SPR data and for managing the ExSAR data, Joanna Grudzinska-Göbel and Ricarda Finnern (Bayer AG) for fruitful discussions, Christian Stegmann (Bayer AG) for complex-formation before crystallization, Dieter Moosmayer (Bayer AG) for recombinant expression and purification of rabbit FXI, Adrian Tersteegen (Bayer AG) for IC_{50} determination of different proteases and Michael Strerath (Bayer AG) for technical support during the screening phase.

Declaration of Interest

M.S., A.B., F.D., J.S., and A.W. are employees of Bayer AG, which provided funding for this study. All authors are also authors of the patent entitled: 'Antibodies capable of binding to the coagulation factor XI and/or its activated form Factor XIa and uses thereof' (number WO2013/167669A1).

Appendix A. Supplementary data

Supplementary data to this article can be found online at https://doi.org/10.1016/j.jmb.2019.09.008.

Received 11 March 2019;
Received in revised form 26 July 2019;
Accepted 10 September 2019
Available online 24 October 2019

Keywords:
Anticoagulant;
Phage display;
Binding epitope;
X-ray structure;
Allosteric mechanism

Abbreviations used:
FXI, factor XI; FXIa, factor XIa; FXa, factor Xa; FIX, factor IX; FXIIa, factor XIIa; VTE, venous thromboembolism; ASO, antisense oligonucleotide; FXIa CD, FXIa catalytic domain; aPTT, activated partial thromboplastin time; A1−A4, Apple 1−4 domains; CDR, complementarity-determining regions; HEK293 cells, human embryonic kidney 293 cells; Fab, fragment antigen binding; VH, variable heavy; VL, variable light; H/D exchange, hydrogen/deuterium exchange; X-ray structure, crystal structure; ELISA, enzyme-linked immunosorbent assay; SPR, Surface Plasmon Resonance.

References

[1] T.B. Larsen, F. Skjøth, P.B. Nielsen, J.N. Kjældgaard, G.Y.H. Lip, Comparative effectiveness and safety of non-vitamin K antagonist oral anticoagulants and warfarin in patients with atrial fibrillation: propensity weighted nationwide cohort study, BMJ 353 (2016), https://doi.org/10.1136/bmj.i3189.

[2] J.I. Weitz, J.C. Fredenburgh, Factors XI and XII as targets for new anticoagulants, Front. Med. 4 (2017) 19.

[3] J.I. Weitz, J.C. Fredenburgh, 2017 scientific sessions Sol Sherry distinguished lecture in thrombosis: factor XI as a target for new anticoagulants, Arterioscler. Thromb. Vasc. Biol. 38 (2018) 304–310.
[4] D. Gailani, S.B. Smith, Structural and functional features of factor XI, J. Thromb. Haemost. 7 (Suppl 1) (2009) 75–78.
[5] D. Gailani, G.J. Broze Jr., Factor XI activation in a revised model of blood coagulation, Science 253 (1991) 909–912.
[6] D. Gailani, T. Renné, Intrinsic pathway of coagulation and arterial thrombosis, Arterioscler. Thromb. Vasc. Biol. 27 (2007) 2507–2513.
[7] B.M. Mohammed, A. Matafonov, I. Ivanov, M.F. Sun, Q. Cheng, S.K. Dickeson, C. Li, D. Sun, I.M. Verhamme, J. Emsley, D. Gailani, An update on factor XI structure and function, Thromb. Res. 161 (2018) 94–105.
[8] D. Gailani, C.E. Bane, A. Gruber, Factor XI and contact activation as targets for antithrombotic therapy, J. Thromb. Haemost. 13 (2015) 1383–1395.
[9] S.B. Smith, D. Gailani, Update on the physiology and pathology of factor IX activation by factor XIa, Expert Rev. Hematol. 1 (2008) 87–98.
[10] O. Salomon, D.M. Steinberg, M. Zucker, D. Varon, A. Zivelin, U. Seligsohn, Patients with severe factor XI deficiency have a reduced incidence of deep-vein thrombosis, Thromb. Haemost. 105 (2011) 269–273.
[11] O. Salomon, D.M. Steinberg, N. Koren-Morag, D. Tanne, U. Seligsohn, Reduced incidence of ischemic stroke in patients with severe factor XI deficiency, Blood 111 (2008) 4113–4117.
[12] S. Duga, O. Salomon, Congenital factor XI deficiency: an update, Semin. Thromb. Hemost. 39 (2013) 621–631.
[13] K. Gomez, P. Bolton-Maggs, Factor XI deficiency, Haemophilia 14 (2008) 1183–1189.
[14] J.C. Meijers, W.L. Tekelenburg, B.N. Bouma, R.M. Bertina, F.R. Rosendaal, High levels of coagulation factor XI as a risk factor for venous thrombosis, N. Engl. J. Med. 342 (2000) 696–701.
[15] M.F. Suri, K. Yamagishi, N. Aleksic, P.J. Hannan, A.R. Folsom, Novel hemostatic factor levels and risk of ischemic stroke: the Atherosclerosis Risk in Communities (ARIC) Study, Cerebrovasc. Dis. 29 (2010) 497–502.
[16] A. Undas, A. Slowik, M. Gissel, K.G. Mann, S. Butenas, Circulating activated factor XI and active tissue factor as predictors of worse prognosis in patients following ischemic cerebrovascular events, Thromb. Res. 128 (2011) e62–e66.
[17] A. Undas, A. Slowik, M. Gissel, K.G. Mann, S. Butenas, Active tissue factor and activated factor XI in patients with acute ischemic cerebrovascular events, Eur. J. Clin. Investig. 42 (2012) 123–129.
[18] Q. Cheng, E.I. Tucker, M.S. Pine, I. Sisler, A. Matafonov, M.F. Sun, T.C. White-Adams, S.A. Smith, S.R. Hanson, O.J. McCarty, T. Renne, A. Gruber, D. Gailani, A role for factor XIIa-mediated factor XI activation in thrombus formation in vivo, Blood 116 (2010) 3981–3989.
[19] X. Wang, Q. Cheng, L. Xu, G.Z. Feuerstein, M.Y. Hsu, P.L. Smith, D.A. Seiffert, W.A. Schumacher, M.L. Ogletree, D. Gailani, Effects of factor IX or factor XI deficiency on ferric chloride-induced carotid artery occlusion in mice, J. Thromb. Haemost. 3 (2005) 695–702.
[20] X. Wang, P.L. Smith, M.Y. Hsu, D. Gailani, W.A. Schumacher, M.L. Ogletree, D.A. Seiffert, Effects of factor XI deficiency on ferric chloride-induced vena cava thrombosis in mice, J. Thromb. Haemost. 4 (2006) 1982–1988.
[21] J.R. Crosby, U. Marzec, A.S. Revenko, C. Zhao, D. Gao, A. Matafonov, D. Gailani, A.R. MacLeod, E.I. Tucker, A. Gruber, S.R. Hanson, B.P. Monia, Antithrombotic effect of antisense factor XI oligonucleotide treatment in primates, Arterioscler. Thromb. Vasc. Biol. 33 (2013) 1670–1678.
[22] J.W. Yau, P. Liao, J.C. Fredenburgh, A.R. Stafford, A.S. Revenko, B.P. Monia, J.I. Weitz, Selective depletion of factor XI or factor XII with antisense oligonucleotides attenuates catheter thrombosis in rabbits, Blood 123 (2014) 2102–2107.
[23] H.S. Younis, J. Crosby, J.I. Huh, H.S. Lee, S. Rime, B. Monia, S.P. Henry, Antisense inhibition of coagulation factor XI prolongs APTT without increased bleeding risk in cynomolgus monkeys, Blood 119 (2012) 2401–2408.
[24] H. Zhang, E.C. Lowenberg, J.R. Crosby, A.R. MacLeod, C. Zhao, D. Gao, C. Black, A.S. Revenko, J.C. Meijers, E.S. Stroes, M. Levi, B.P. Monia, Inhibition of the intrinsic coagulation pathway factor XI by antisense oligonucleotides: a novel antithrombotic strategy with lowered bleeding risk, Blood 116 (2010) 4684–4692.
[25] T. David, Y.C. Kim, L.K. Ely, I. Rondon, H. Gao, P. O'Brien, M.W. Bolt, A.J. Coyle, J.L. Garcia, E.A. Flounders, T. Mikita, S.R. Coughlin, Factor XIa-specific IgG and a reversal agent to probe factor XI function in thrombosis and hemostasis, Sci. Transl. Med. 8 (2016), 353ra112.
[26] E.I. Tucker, U.M. Marzec, T.C. White, S. Hurst, S. Rugonyi, O.J. McCarty, D. Gailani, A. Gruber, S.R. Hanson, Prevention of vascular graft occlusion and thrombus-associated thrombin generation by inhibition of factor XI, Blood 113 (2009) 936–944.
[27] A. Yamashita, K. Nishihira, T. Kitazawa, K. Yoshihashi, T. Soeda, K. Esaki, T. Imamura, K. Hattori, Y. Asada, Factor XI contributes to thrombus propagation on injured neointima of the rabbit iliac artery, J. Thromb. Haemost. 4 (2006) 1496–1501.
[28] M.L. van Montfoort, V.L. Knaup, J.A. Marquart, K. Bakhtiari, F.J. Castellino, C.E. Hack, J.C. Meijers, Two novel inhibitory anti-human factor XI antibodies prevent cessation of blood flow in a murine venous thrombosis model, Thromb. Haemost. 110 (2013) 1065–1073.
[29] L.K. Ely, M. Lolicato, T. David, K. Lowe, Y.C. Kim, D. Samuel, P. Bessette, J.L. Garcia, T. Mikita, D.L. Minor Jr., S.R. Coughlin, Structural basis for activity and specificity of an anticoagulant anti-FXIa monoclonal antibody and a reversal agent, Structure 26 (2018), 187–198.e4.
[30] H.R. Buller, C. Bethune, S. Bhanot, D. Gailani, B.P. Monia, G.E. Raskob, A. Segers, P. Verhamme, J.I. Weitz, Factor XI antisense oligonucleotide for prevention of venous thrombosis, N. Engl. J. Med. 372 (2015) 232–240.
[31] S. Hanessian, A. Larsson, T. Fex, W. Knecht, N. Blomberg, Design and synthesis of macrocyclic indoles targeting blood coagulation cascade factor XIa, Bioorg. Med. Chem. Lett 20 (2010) 6925–6928.
[32] H. Deng, T.D. Bannister, L. Jin, R.E. Babine, J. Quinn, P. Nagafuji, C.A. Celatka, J. Lin, T.I. Lazarova, M.J. Rynkiewicz, F. Bibbins, P. Pandey, J. Gorga, H.V. Meyers, S.S. Abdel-Meguid, J.E. Strickler, Synthesis, SAR exploration, and X-ray crystal structures of factor XIa inhibitors containing an alpha-ketothiazole arginine, Bioorg. Med. Chem. Lett 16 (2006) 3049–3054.
[33] T.I. Lazarova, L. Jin, M. Rynkiewicz, J.C. Gorga, F. Bibbins, H.V. Meyers, R. Babine, J. Strickler, Synthesis and in vitro biological evaluation of aryl boronic acids as potential

inhibitors of factor XIa, Bioorg. Med. Chem. Lett 16 (2006) 5022–5027.
[34] M.S. Buchanan, A.R. Carroll, D. Wessling, M. Jobling, V.M. Avery, R.A. Davis, Y. Feng, Y. Xue, L. Oster, T. Fex, J. Deinum, J.N. Hooper, R.J. Quinn, Clavatadine A, a natural product with selective recognition and irreversible inhibition of factor XIa, J. Med. Chem. 51 (2008) 3583–3587.
[35] M.L. Quan, P.C. Wong, C. Wang, F. Woerner, J.M. Smallheer, F.A. Barbera, J.M. Bozarth, R.L. Brown, M.R. Harpel, J.M. Luettgen, P.E. Morin, T. Peterson, V. Ramamurthy, A.R. Rendina, K.A. Rossi, C.A. Watson, A. Wei, G. Zhang, D. Seiffert, R.R. Wexler, Tetrahydroquinoline derivatives as potent and selective factor XIa inhibitors, J. Med. Chem. 57 (2014) 955–969.
[36] P.C. Wong, E.J. Crain, C.A. Watson, W.A. Schumacher, A small-molecule factor XIa inhibitor produces antithrombotic efficacy with minimal bleeding time prolongation in rabbits, J. Thromb. Thrombolysis 32 (2011) 129–137.
[37] R. Karuturi, R.A. Al-Horani, S.C. Mehta, D. Gailani, U.R. Desai, Discovery of allosteric modulators of factor XIa by targeting hydrophobic domains adjacent to its heparin-binding site, J. Med. Chem. 56 (2013) 2415–2428.
[38] R.A. Al-Horani, P. Ponnusamy, A.Y. Mehta, D. Gailani, U.R. Desai, Sulfated pentagalloylglucoside is a potent, allosteric, and selective inhibitor of factor XIa, J. Med. Chem. 56 (2013) 867–878.
[39] M.D. Argade, A.Y. Mehta, A. Sarkar, U.R. Desai, Allosteric inhibition of human factor XIa: discovery of monosulfated benzofurans as a class of promising inhibitors, J. Med. Chem. 57 (2014) 3559–3569.
[40] X. Fradera, B. Kazemier, E. Carswell, A. Cooke, A. Oubrie, W. Hamilton, M. Dempster, S. Krapp, S. Nagel, A. Jestel, High-resolution crystal structures of factor XIa coagulation factor in complex with nonbasic high-affinity synthetic inhibitors, Acta Crystallogr. Sect. F Struct. Biol. Cryst. Commun. 68 (2012) 404–408.
[41] L. Jin, P. Pandey, R.E. Babine, D.T. Weaver, S.S. Abdel-Meguid, J.E. Strickler, Mutation of surface residues to promote crystallization of activated factor XI as a complex with benzamidine: an essential step for the iterative structure-based design of factor XI inhibitors, Acta Crystallogr. D Biol. Crystallogr. 61 (2005) 1418–1425.
[42] J. Emsley, P.A. McEwan, D. Gailani, Structure and function of factor XI, Blood 115 (2010) 2569–2577.
[43] B.A. McMullen, K. Fujikawa, E.W. Davie, Location of the disulfide bonds in human coagulation factor XI: the presence of tandem apple domains, Biochemistry 30 (1991) 2056–2060.
[44] J.C. Meijers, E.W. Davie, D.W. Chung, Expression of human blood coagulation factor XI: characterization of the defect in factor XI type III deficiency, Blood 79 (1992) 1435–1440.
[45] R. He, D. Chen, S. He, Factor XI: hemostasis, thrombosis, and antithrombosis, Thromb. Res. 129 (2012) 541–550.
[46] K.O. Badellino, P.N. Walsh, Localization of a heparin binding site in the catalytic domain of factor XIa, Biochemistry 40 (2001) 7569–7580.
[47] L. Yang, M.F. Sun, D. Gailani, A.R. Rezaie, Characterization of a heparin-binding site on the catalytic domain of factor XIa: mechanism of heparin acceleration of factor XIa inhibition by the serpins antithrombin and C1-inhibitor, Biochemistry 48 (2009) 1517–1524.
[48] F.A. Baglia, P.N. Walsh, A binding site for thrombin in the apple 1 domain of factor XI, J. Biol. Chem. 271 (1996) 3652–3658.
[49] T. Renne, D. Gailani, J.C. Meijers, W. Muller-Esterl, Characterization of the H-kininogen-binding site on factor XI: a comparison of factor XI and plasma prekallikrein, J. Biol. Chem. 277 (2002) 4892–4899.
[50] M.F. Sun, M. Zhao, D. Gailani, Identification of amino acids in the factor XI apple 3 domain required for activation of factor IX, J. Biol. Chem. 274 (1999) 36373–36378.
[51] F.A. Baglia, D. Gailani, J.A. Lopez, P.N. Walsh, Identification of a binding site for glycoprotein Ibalpha in the Apple 3 domain of factor XI, J. Biol. Chem. 279 (2004) 45470–45476.
[52] D.H. Ho, K. Badellino, F.A. Baglia, P.N. Walsh, A binding site for heparin in the apple 3 domain of factor XI, J. Biol. Chem. 273 (1998) 16382–16390.
[53] M. Zhao, T. Abdel-Razek, M.F. Sun, D. Gailani, Characterization of a heparin binding site on the heavy chain of factor XI, J. Biol. Chem. 273 (1998) 31153–31159.
[54] F.A. Baglia, B.A. Jameson, P.N. Walsh, Identification and characterization of a binding site for factor XIIa in the Apple 4 domain of coagulation factor XI, J. Biol. Chem. 268 (1993) 3838–3844.
[55] W. Wu, D. Sinha, S. Shikov, C.K. Yip, T. Walz, P.C. Billings, J.D. Lear, P.N. Walsh, Factor XI homodimer structure is essential for normal proteolytic activation by factor XIIa, thrombin, and factor XIa, J. Biol. Chem. 283 (2008) 18655–18664.
[56] M. Zucker, A. Zivelin, M. Landau, N. Rosenberg, U. Seligsohn, Three residues at the interface of factor XI (FXI) monomers augment covalent dimerization of FXI, J. Thromb. Haemost. 7 (2009) 970–975.
[57] D. Gailani, Y. Geng, I. Verhamme, M.F. Sun, S.P. Bajaj, A. Messer, J. Emsley, The mechanism underlying activation of factor IX by factor XIa, Thromb. Res. 133 (Suppl. 1) (2014) S48–S51.
[58] Y. Geng, I.M. Verhamme, S.B. Smith, M.F. Sun, A. Matafonov, Q. Cheng, S.A. Smith, J.H. Morrissey, D. Gailani, The dimeric structure of factor XI and zymogen activation, Blood 121 (2013) 3962–3969.
[59] E. Papagrigoriou, P.A. McEwan, P.N. Walsh, J. Emsley, Crystal structure of the factor XI zymogen reveals a pathway for transactivation, Nat. Struct. Mol. Biol. 13 (2006) 557–558.
[60] R.M. Hoet, E.H. Cohen, R.B. Kent, K. Rookey, S. Schoonbroodt, S. Hogan, L. Rem, N. Frans, M. Daukandt, H. Pieters, R. van Hegelsom, N.C. Neer, H.G. Nastri, I.J. Rondon, J.A. Leeds, S.E. Hufton, L. Huang, I. Kashin, M. Devlin, G. Kuang, M. Steukers, M. Viswanathan, A.E. Nixon, D.J. Sexton, H.R. Hoogenboom, R.C. Ladner, Generation of high-affinity human antibodies by combining donor-derived and synthetic complementarity-determining-region diversity, Nat. Biotechnol. 23 (2005) 344–348.
[61] D. Navaneetham, L. Jin, P. Pandey, J.E. Strickler, R.E. Babine, S.S. Abdel-Meguid, P.N. Walsh, Structural and mutational analyses of the molecular interactions between the catalytic domain of factor XIa and the Kunitz protease inhibitor domain of protease nexin 2, J. Biol. Chem. 280 (2005) 36165–36175.
[62] R.A. Al-Horani, U.R. Desai, Designing allosteric inhibitors of factor XIa. Lessons from the interactions of sulfated pentagalloylglucopyranosides, J. Med. Chem. 57 (2014) 4805–4818.
[63] B.N. Bouma, J.H. Griffin, Human blood coagulation factor XI. Purification, properties, and mechanism of activation by activated factor XII, J. Biol. Chem. 252 (1977) 6432–6437.

[64] S.B. Smith, I.M. Verhamme, M.F. Sun, P.E. Bock, D. Gailani, Characterization of novel forms of coagulation factor XIa: independence of factor XIa subunits in factor IX activation, J. Biol. Chem. 283 (2008) 6696–6705.
[65] T. Mikita, L.K. Ely, H. Gao, Y. Kim, I. Rondon, T. David, S.R. Coughlin, Antibodies to Coagulation Factor FXIa and Uses Thereof, Pfizer, 2017.
[66] P. Wong, C. Kettner, L. Mersinger, C. Watson, E. Crain, M. Harpel, W. Schumacher, M. Ogletree, A. Rendina, Nonpeptide Factor XIa Inhibitor. In Vitro Kinetic Evaluation and In Vivo Studies of BMS-262084 On Arterial Thrombosis and Hemostasis in Rabbits, 2010. Poster P2316 presented at European Society of Cardiology Congress, Stockholm, Sweden on Monday 30 August 2010. Available at: http://spo.escardio.org/eslides/view.aspx?eevtid=40&fp=P2316. (Accessed 11 September 2018).
[67] E.P. Feener, Q. Zhou, W. Fickweiler, Role of plasma kallikrein in diabetes and metabolism, Thromb. Haemost. 110 (2013) 434–441.
[68] J.I. Weitz, Factor XI and factor XII as targets for new anticoagulants, Thromb. Res. 141 (Suppl. 2) (2016) S40–S45.
[69] R. Tom, L. Bisson, Y. Durocher, Transient expression in HEK293-EBNA1 cells, in: M.R. Dyson, Y. Durocher (Eds.), Methods Express: Expression Systems, Scion Publishing Ltd., Oxfordshire, UK, 2007.
[70] Y. Durocher, S. Perret, A. Kamen, High-level and high-throughput recombinant protein production by transient transfection of suspension-growing human 293-EBNA1 cells, Nucleic Acids Res. 30 (2002) E9.
[71] W. Kabsch, XDS, Acta Crystallogr. D Biol. Crystallogr. 66 (2010) 125–132.
[72] P.R. Evans, An introduction to data reduction: space-group determination, scaling and intensity statistics, Acta Crystallogr. D Biol. Crystallogr. 67 (2011) 282–292.
[73] P. Evans, Scaling and assessment of data quality, Acta Crystallogr. D Biol. Crystallogr. 62 (2006) 72–82.
[74] F. Long, A.A. Vagin, P. Young, G.N. Murshudov, BALBES: a molecular-replacement pipeline, Acta Crystallogr. D Biol. Crystallogr. 64 (2008) 125–132.
[75] A. Vagin, A. Teplyakov, Molecular replacement with MOLREP, Acta Crystallogr. D Biol. Crystallogr. 66 (2010) 22–25.
[76] G.N. Murshudov, A.A. Vagin, E.J. Dodson, Refinement of macromolecular structures by the maximum-likelihood method, Acta Crystallogr. D Biol. Crystallogr. 53 (1997) 240–255.
[77] P. Emsley, B. Lohkamp, W.G. Scott, K. Cowtan, Features and development of coot, Acta Crystallogr. D Biol. Crystallogr. 66 (2010) 486–501.
[78] L.L.C. Schrodinger, The PyMOL Molecular Graphics System, 2015, Version 1.8.
[79] P. Briggs, An Informal Newsletter Associated With the BBSRC Collaborative Computational Project No. 4 on Protein Crystallography, Number 38, April 2000. Available at: http://www.ccp4.ac.uk/newsletters/newsletter38/00_contents.html. (Accessed 25 April 2018).
[80] A.J. Percy, M. Rey, K.M. Burns, D.C. Schriemer, Probing protein interactions with hydrogen/deuterium exchange and mass spectrometry-a review, Anal. Chim. Acta 721 (2012) 7–21.
[81] H.C. Hemker, P. Giesen, R. Al Dieri, V. Regnault, E. de Smedt, R. Wagenvoord, T. Lecompte, S. Beguin, Calibrated automated thrombin generation measurement in clotting plasma, Pathophysiol. Haemost. Thromb. 33 (2003) 4–15.